Magnetic ground state of FeSe

Qisi Wang,[1†] Yao Shen,[1†] Bingying Pan,[1†] Xiaowen Zhang,[1] K. Ikeuchi,[2] K. Iida,[2] A. D. Christianson,[3, 4] H. C. Walker,[5]

D. T. Adroja,[5] M. Abdel-Hafiez,[6, 7] Xiaojia Chen,[6] D. A. Chareev,[8] A. N. Vasiliev,[9, 10, 11] and Jun Zhao[*1, 12]

[1] *State Key Laboratory of Surface Physics and Department of Physics, Fudan University, Shanghai 200433, China*

[2] *Research Center for Neutron Science and Technology, Comprehensive Research Organization for Science and Society, Tokai, Ibaraki 319-1106, Japan*

[3] *Quantum Condensed Matter Division, Oak Ridge National Laboratory, Oak Ridge, Tennessee 37831, USA*

[4] *Department of Physics and Astronomy, University of Tennessee, Knoxville, Tennessee 37996, USA*

[5] *ISIS Facility, Rutherford Appleton Laboratory, STFC, Chilton, Didcot, Oxon OX11 0QX, United Kingdom*

[6] *Center for High Pressure Science and Technology Advanced Research, Shanghai, 201203, China*

[7] *Faculty of Science, Physics Department, Fayoum University, 63514 Fayoum, Egypt*

[8] *Institute of Experimental Mineralogy, Russian Academy of Sciences, 142432 Chernogolovka, Moscow District, Russia*

[9] *Low Temperature Physics and Superconductivity Department,*

M.V. Lomonosov Moscow State University, 119991 Moscow, Russia

[10] *Theoretical Physics and Applied Mathematics Department, Ural Federal University, 620002 Ekaterinburg, Russia*

[11] *National University of Science and Technology "MISiS", Moscow 119049, Russia*

[12] *Collaborative Innovation Center of Advanced Microstructures, Fudan University, Shanghai 200433, China*

[†] These authors contribute equally to this work.
[*] Correspondence and requests for materials should be addressed to J.Z. (zhaoj@fudan.edu.cn).

Elucidating the nature of the magnetism of a high-temperature superconductor is crucial for establishing its pairing mechanism[1]. **The parent compounds of the cuprate and iron-pnictide superconductors exhibit Néel and stripe magnetic order, respectively**[1,2]**. However, FeSe, the structurally simplest and one of the most intriguing iron-based superconductors, shows nematic order (T_s = 90 K), but not magnetic order in the parent phase**[3]**, and its magnetic ground state is intensely debated**[4–8]**. Here, we report inelastic neutron-scattering experiments that reveal both stripe and Néel spin fluctuations over a wide energy range at 110 K. On entering the nematic phase, a substantial amount of spectral weight is transferred from the Néel to the stripe spin fluctuations, which results in a ~ 30 meV gap in the Néel spin fluctuations. Moreover, although the spin-fluctuation bandwidth is lower, the total fluctuating magnetic moment ($\langle m^2 \rangle$ = 5.19 μ_B^2/Fe) of FeSe is ~ 60% larger than that in the iron pnictide BaFe$_2$As$_2$ (ref. 9). These results indicate that FeSe is an S = 1 nematic quantum-disordered paramagnet interpolating between the Néel and stripe magnetic instabilities**[4]**. Thus, our findings reveal an unexpected connection between the magnetism of the cuprate- and iron-based superconductors, and also imply that the Néel spin fluctuations might be relevant to the unique superconducting properties of FeSe, including its drastically enhanced superconductivity under pressure, through electron doping or in the mono layer limit**[10–13]**.**

Recently, FeSe has attracted considerable interest because of its atypical magnetism and fascinating superconducting properties. Although the superconducting transition temperature T_c of bulk FeSe (T_c ≈ 8 K) is low, it increases drastically under pressure (T_c ≈ 37 K; ref. 10), by carrier doping (T_c ≈ 40-

48 K; refs 11, 12), or in the mono layer limit ($T_c \sim$ 65-100 K, ref. 13). The unique superconducting properties of FeSe are presumably related to its magnetic ground state, which remains undetermined[4–8]. We used inelastic neutron scattering to study the spin fluctuations of single crystalline FeSe (see Methods). Figure 1 shows the constant-energy images of spin fluctuations in the (H, K) plane. Here, in the high temperature tetragonal phase (110 K), the spin response is strongest at $\mathbf{Q} = (1, 0)$ at 15 meV (Fig. 1a), which is consistent with previous low energy measurements[14,15]. With an increase in energy (Fig. 1b-g), the spin fluctuations show anisotropic dispersion and counter-propagate mainly along the K direction. This is analogous to the stripe spin fluctuations detected in other iron based superconductors[1,9,16]. Most notably, in addition to the stripe spin fluctuations, comparatively weaker but clear scattering appears near (1, 1), which implies the presence of spin fluctuations associated with the Néel magnetic instability (see Methods); different from the anisotropic stripe spin fluctuations, the Néel spin fluctuations are nearly isotropic in the transverse and longitudinal directions. With an increase in the energy up to approximately 150 meV, the Néel and stripe spin fluctuations overlap and cover a broad area centred at (1, 1) (Fig. 1h). Upon cooling to within the nematic phase ($T = 4$ K), the Néel spin-fluctuation signal weakens considerably and is almost undetectable below 35 meV (Fig. 1i, 1j). On the other hand, the momentum structure of the stripe spin fluctuation is essentially unchanged above and below T_s.

To further elucidate the spin fluctuations in E-$\mathbf{Q}$ space, we projected the spin fluctuations along the K direction near (1, 0) and (1, 1) (Fig. 2). As shown in Fig. 2a, the stripe spin fluctuations stem from (1, 0), split into two branches at ~35 meV and extend up to above ~150 meV at 110 K. The steeply dispersive Néel spin fluctuations are also visible (green arrowheads). As the temperature is lowered

to 4 K, the Néel spin fluctuation exhibits a ~ 30 meV gap while the stripe spin fluctuations below 70 meV are clearly enhanced (Fig. 2b).

To quantify the dispersions and intensities of the stripe and Néel spin fluctuations, we made constant-energy cuts at distinct energies (Fig. 3). As Fig. 3c-h show, at $T = 110$ K, the single peak centred at $(1, 0)$ at 15 meV evolves into a pair of peaks along the K direction at $E \geq 35$ meV. By contrast, the peak position of the Néel spin fluctuation (see green arrowheads) shows little change; it only broadens gradually in wavevector with increasing energy. The Néel spin fluctuation is more clearly visible along the transverse direction (Fig. 3k-p) because of the comparatively weaker influence of the stripe spin fluctuations. Here, double peaks formed due to the dispersion are not seen below 68 meV, because the Néel spin fluctuations are commensurate and steeply dispersive (Fig. 3k-p). At higher energies, the Néel and stripe spin fluctuation spectra merge with each other, and their dispersions cannot be determined unambiguously (Fig. 3a, 3b, 3i, 3j). The Néel spin fluctuation becomes featureless at low energies (Fig. 3h, 3p) at 4 K, which agrees with the results shown in the constant-energy and E-$\mathbf{Q}$ images (Fig. 1i, 2b). We attempted to fit both types of spectra concurrently using a linear spin-wave theory for the two neighbour ($J_{1(a/b)}$-J_2) or three neighbour ($J_{1(a/b)}$-J_2-J_3) Heisenberg model, where $J_{1(a/b)}$, J_2 and J_3 are nearest neighbor (in the a/b direction), next nearest neighbour and next next nearest neighbour exchange coupling constants, respectively; but this was unsuccessful mainly because this theory cannot account for the observed strong low energy spin excitations at both $(1, 0)$ and $(1, 1)$.

More insight into the nature of the underlying magnetic ground state and its interaction with the nematicity could be acquired by calculating in absolute units the energy dependence of the momentum integrated local susceptibility $\chi''(\omega)$ above and below T_s; as Fig. 4a and 4b show, at $T = $ 110 K, the Néel spin fluctuation spectral weight is roughly 26% of that of the stripe spin fluctuation below 52 meV, where the two signals are well separated in q-space. Upon cooling to $T = 4$ K, the spectral weight loss for the Néel spin fluctuations is approximately recovered by the enhanced stripe spin fluctuations (red shaded areas), and thus the total local susceptibility $\chi''(\omega)$ does not show a marked change across T_s (Fig. 4c). Moreover, the detailed temperature dependence of the stripe and Néel spin fluctuations show that the spectral weight transfer is clearly coupled with the development of the nematic phase (Fig. 4d). At both 4 and 110 K, the total $\chi''(\omega)$ exhibits a high maximum at ~105 meV and extends up to 220 meV (Fig. 3a, 3b, 4c). This bandwidth is considerably lower than that (~ 340 meV) of the stripe ordered $BaFe_2As_2$ (ref. 9), which is very likely due to the competition between the Néel and stripe magnetic instabilities. Clearly, this type of competition also prevents the long-range magnetic order in FeSe. By integrating the spectral weight from low energy to the zone boundary, we determined that the total fluctuating moment at 4 K and 110 K are $\langle m^2 \rangle = (g\mu_B)^2 S(S + 1) = 5.19 \pm 0.32$ and 5.12 ± 0.27 μ_B^2/Fe, respectively, which are larger than those in the superconducting $BaFe_{1.9}Ni_{0.1}As_2$ ($\langle m^2 \rangle = 3.2$ μ_B^2/Fe) and stripe ordered $BaFe_2As_2$ ($\langle m^2 \rangle = 3.17$ μ_B^2/Fe) (ref. 9). Accordingly, this yields an effective spin of $S \approx 0.74$ in FeSe, which likely corresponds to an $S = 1$ ground state in the presence of itinerant electrons.

The coexistence of the Néel and stripe spin fluctuations is unexpected because FeSe contains only one type of magnetic ions. Although density functional theory and dynamical mean field theory

failed to reproduce the observed band structure of FeSe (refs 17,18), a random phase approximation

calculation with an "engineered" tight-binding band structure[19] predicted the spin fluctuations near

(1, 0) and (1, q). However, in this phenomenological model[19], the (1, q) spin fluctuation is

incommensurate and gapless below T_s, which is inconsistent with our data. The relatively small spin-

fluctuation bandwidth and large fluctuating moment together with the low carrier density[17,18] indicate

that the magnetic moments in FeSe are more localised than in iron pnictides.

In the more localised case, we can exclude the previously proposed competing staggered

dimer/trimers/tetramers magnetic order[5] and pair-checkerboard order[7]. Here, the competition

between the Néel and stripe magnetic instabilities could be instead understood within the framework

of a frustrated J_1-J_2 model. In this model, the Néel order is stable for $J_2/J_1 \lesssim 0.4$, which is

appropriate for the cuprates, whereas the stripe order is the ground state for $0.6 \lesssim J_2/J_1$ (refs 20,21).

It was predicted that FeSe would be an $S = 1$ nematic quantum paramagnet in the intermediate

coupling region ($0.4 \lesssim J_2/J_1 \lesssim 0.6$), which is characterized by gapped stripe and Néel spin

fluctuations[4]. This agrees with our data that the majority of the spectral weight is concentrated at

relatively high energies (~100 meV) even in the presence of itinerant electrons (Fig. 2a, 2b and 4c).

Furthermore, in this scenario, the nematic order is viewed as a "vestigial" order that is retained when

the static stripe order is suppressed by quantum fluctuations[4]. The finding that the stripe spin

fluctuation carries considerably more spectral weight than the Néel spin fluctuation suggests that the

system is indeed closer to stripe rather than to Néel order. On this basis, the temperature evolution of

the spin fluctuations that we observed can be explained. As the stripe magnetic order breaks the C_4

lattice symmetry, while the Néel order preserves it, the orthorhombic/nematic phase transition might

partially lift the magnetic frustration and drive the system toward the stripe ordered phase. Thus, the stripe spin fluctuations are enhanced while the Néel spin fluctuations are suppressed and gapped in the nematic phase. These considerations lead to a natural understanding of the paramagnetic nematic phase in FeSe.

Finally, we discuss the evolution of the nematicity, magnetism and superconductivity in FeSe and its derivatives. The competition between the Néel and stripe magnetic instabilities suggests a highly tunable magnetic ground state in FeSe. Indeed, it has been shown that high pressure ($P > \sim 1.8$ GPa) not only enhances the superconductivity, but also induces static magnetic order while completely suppressing the nematicity/ orthorhombicity in FeSe (refs 22,23). This is most likely the Néel type magnetic order rather than the stripe type, because the stripe order is incompatible with the tetragonal structure. Therefore, the enhanced Néel spin correlations could be relevant to the increase of T_c under pressure. In addition, the presence of the Néel spin fluctuations might also have implications for our understanding of the drastically enhanced superconductivity in the K dosed[12,24], molecule intercalated[25] and mono layer[13,26] FeSe, because in these heavily electron doped compounds, the nematic order and the hole pockets are absent, and the electron pockets at two separated zone edges are connected by the Néel wavevector $\mathbf{Q}= (1, 1)$. This may, in turn, make the Néel spin fluctuations and Fermi surfaces interact synergistically to enhance superconductivity[27–29]. Interestingly, this would be in analogy with the cuprate superconductors in terms of the magnetism and Fermi surface topology[2]. To further elucidate the role of the Néel spin fluctuations in iron-based superconductivity, a detailed study of the pressure/electron-doping dependence of the spin correlations in FeSe would be desirable.

Methods

Our inelastic neutron scattering measurements were carried out on the ARCS time-of-flight chopper spectrometer at the Spallation Neutron Source of Oak Ridge National Laboratory, USA, 4SEASONS chopper spectrometer at the Japan Proton Accelerator Research Complex (J-PARC), and MERLIN chopper spectrometer at the Rutherford Appleton Laboratory, Didcot, UK. The large detector arrays on these instruments allowed us to measure spin excitations over a wide range of energy and momentum. In order to facilitate comparison with theory and previous measurements, our data were normalised into absolute units by using the elastic incoherent scattering of a standard vanadium sample. The incident neutron beam was aligned parallel to the c axis. The wavevector $\mathbf{Q}$ at (q_x, q_y, q_z) is defined as (H, K, L) = ($q_x a/2\pi$, $q_y b/2\pi$, $q_z c/2\pi$) in the reciprocal lattice units in the orthorhombic unit cell. In this unit cell, the magnetic wavevectors associated with the stripe and Néel magnetic order are $\mathbf{Q} = (1, 0)$ and $\mathbf{Q} = (1, 1)$, which correspond to the ordering wavevectors of the parent compounds of the iron pnictides and the cuprates, respectively. Our FeSe single crystals were grown as reported in ref. 30. The single crystal X-ray diffraction refinements on our sample indicated a stoichiometric chemical composition [$FeSe_{0.990(10)}$] to within the error bar, and no interstitial atoms or impurity phases were observed. Our sample was also characterised by resistivity and susceptibility measurements in ref. 14.

References

1.   Dai, P. C. Antiferromagnetic order and spin dynamics in iron-based superconductors. *Rev. Mod. Phys.* **87,** 855 (2015).

2.   Lee, P. A., Nagaosa, N. & Wen, X. G. Doping a Mott insulator: Physics of high-temperature superconductivity. *Rev. Mod. Phys.* **78,** 17 (2006).

3.   McQueen, T. *et al.* Tetragonal-to-orthorhombic structural phase transition at 90 K in the superconductor Fe1.01Se. *Phys. Rev. Lett.* **103,** 057002 (2009).

4.   Wang, F., Kivelson, S. A. & Lee, D. -H. Nematicity and quantum paramagnetism in FeSe. *Nat. Phys.* (2015). doi:10.1038/nphys3456

5.   Glasbrenner, J. K. *et al.* Effect of magnetic frustration on nematicity and superconductivity in iron chalcogenides. *Nat. Phys.* (2015). doi:10.1038/nphys3434

6.   Yu, R. & Si, Q. Antiferroquadrupolar and Ising-nematic orders of a frustrated bilinear-biquadratic Heisenberg model and implications for the magnetism of FeSe. *Phys. Rev. Lett.* **115,** 116401 (2015).

7.   Cao, H.-Y., Chen, S., Xiang, H. & Gong, X.-G. Antiferromagnetic ground state with pair-checkerboard order in FeSe. *Phys. Rev. B* **91,** 020504(R) (2015).

8. Chubukov, A. V., Fernandes, R. M. & Schmalian, J. Origin of nematic order in FeSe. *Phys. Rev. B* **91,** 201105(R) (2015).

9. Liu, M. *et al.* Nature of magnetic excitations in superconducting $BaFe_{1.9}Ni_{0.1}As_2$. *Nat. Phys.* **8,** 376-381 (2012).

10. Medvedev, S. *et al.* Electronic and magnetic phase diagram of β-$Fe_{1.01}Se$ with superconductivity at 36.7 K under pressure. *Nat. Mater.* **8,** 630–633 (2009).

11. Burrard-Lucas, M. *et al.* Enhancement of the superconducting transition temperature of FeSe by intercalation of a molecular spacer layer. *Nat. Mater.* **12,** 15-19 (2013).

12. Miyata, Y., Nakayama, K., Sugawara, K., Sato, T. & Takahashi, T. High-temperature superconductivity in potassium-coated multilayer FeSe thin films. *Nat. Mater.* **14,** 775-779 (2015).

13. Ge, J.-F. *et al.* Superconductivity above 100 K in single-layer FeSe films on doped $SrTiO_3$. *Nat. Mater.* **14,** 285-289 (2015).

14. Wang, Q. *et al.* Strong interplay between stripe spin fluctuations, nematicity and superconductivity in FeSe. Preprint at <http://arxiv.org/abs/1502.07544> (2015).

15. Rahn, M. C., Ewings, R. A., Sedlmaier, S. J., Clarke, S. J. & Boothroyd, A. T. Strong $(\pi,0)$ spin fluctuations in β-FeSe observed by neutron spectroscopy. *Phys. Rev. B* **91,** 180501(R) (2015).

16. Lumsden, M. D. *et al.* Evolution of spin excitations into the superconducting state in $FeTe_{1-x}Se_x$. *Nat. Phys.* **6,** 182-186 (2010).

17. Watson, M. D. *et al.* Emergence of the nematic electronic state in FeSe. *Phys. Rev. B* **91,** 155106 (2015).

18. Shimojima, T. *et al.* Lifting of xz/yz orbital degeneracy at the structural transition in detwinned FeSe. *Phys. Rev. B* **90,** 121111(R) (2014).

19. Kreisel, A., Mukherjee, S., Hirschfeld, P. J. & Andersen, B. M. Spin excitations in a model of FeSe with orbital ordering. Preprint at <http://arxiv.org/abs/1510.02357> (2015).

20. Sushkov, O. P., Oitmaa, J. & Weihong, Z. Quantum phase transitions in the two-dimensional J_1-J_2 model. *Phys. Rev. B* **63,** 104420 (2001).

21. Jiang, H. C. *et al.* Phase diagram of the frustrated spatially-anisotropic S=1 antiferromagnet on a square lattice. *Phys. Rev. B* **79,** 174409 (2009).

22. Bendele, M. *et al.* Coexistence of superconductivity and magnetism in $FeSe_{1-x}$ under pressure. *Phys. Rev. B* **85,** 064517 (2012).

23. Terashima, T. *et al.* Pressure-induced antiferromagnetic transition and phase diagram in FeSe. *J. Phys. Soc. Jpn.* **84,** 063701 (2015).

24. Wen, C. H. P. *et al.* Anomalous correlation effects and unique phase diagram of electron doped FeSe revealed by angle resolved photoemission spectroscopy. Preprint at <http://arxiv.org/abs/1508.05848> (2015).

25. Zhao, L. *et al.* Common electronic origin of superconductivity in (Li,Fe)OHFeSe bulk superconductor and single-layer $FeSe/SrTiO_3$ films. Preprint at <http://arxiv.org/abs/1505.06361> (2015).

26. Tan, S. *et al.* Interface-induced superconductivity and strain-dependent spin density waves in $FeSe/SrTiO_3$ thin films. *Nat. Mater.* **12,** 634-640 (2013).

27. Davis, J. C. S. & Lee, D.-H. Concepts relating magnetic interactions, intertwined electronic orders, and strongly correlated superconductivity. *Proc. Natl. Acad. Sci. U. S. A.* **110,** 17623-17630 (2013).

28. Hirschfeld, P. J., Korshunov, M. M. & Mazin, I. I. Gap symmetry and structure of Fe-based superconductors. *Reports Prog. Phys.* **74,** 124508 (2011).

29. Lee, D.-H. What makes the T_c of $FeSe/SrTiO_3$ so high? Preprint at <http://arxiv.org/abs/1508.02461> (2015).

30. Chareev, D. *et al.* Single crystal growth and characterization of tetragonal $FeSe_{1-x}$ superconductors. *CrystEngComm* **15,** 1989-1993 (2013).
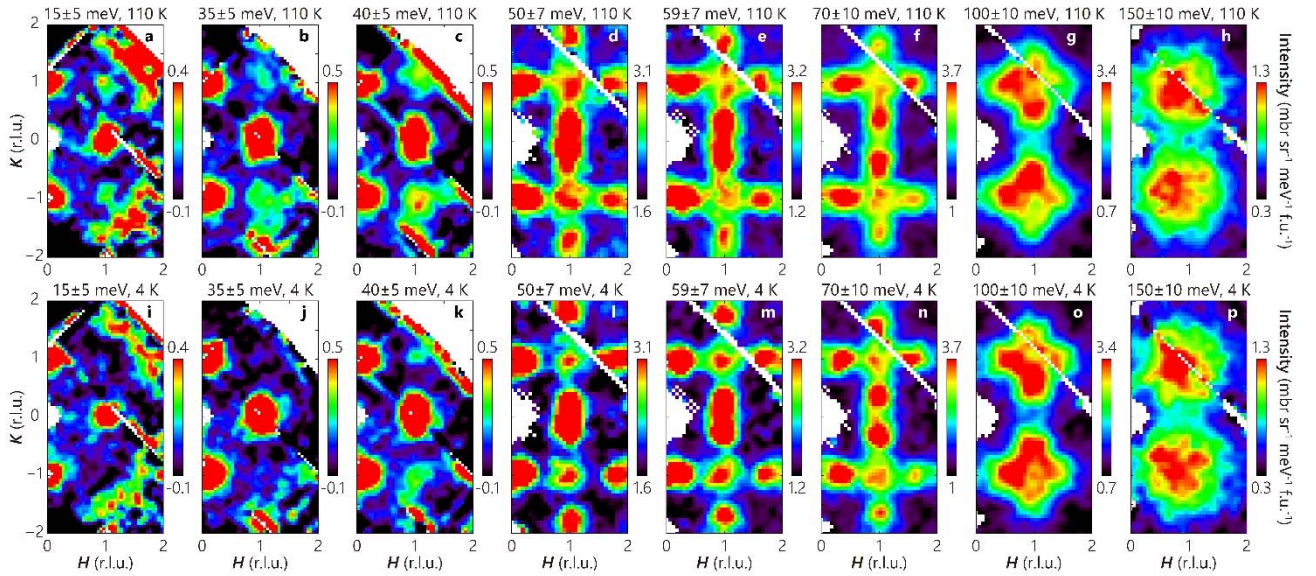
Figure 1 | Momentum dependence of the spin fluctuations in FeSe at 4 K and 110 K. a-h, Constant-energy images acquired at 110 K at indicated energies. **i-p,** Constant-energy images obtained at 4 K at the same intensity scale as those acquired at 110 K. The measurements in (**a-c**, **i-k**) and (**d-h**, **l-p**) were carried out on ARCS with the incident neutron energy of 79 and 294 meV, respectively. Symmetry equivalent data were pooled to enhance statistical accuracy. The |**Q**|-dependent background is subtracted for the data (**a-c**, **i-k**) below the aluminium phonon cutoff energy of ~ 40 meV (see Supplementary Information).
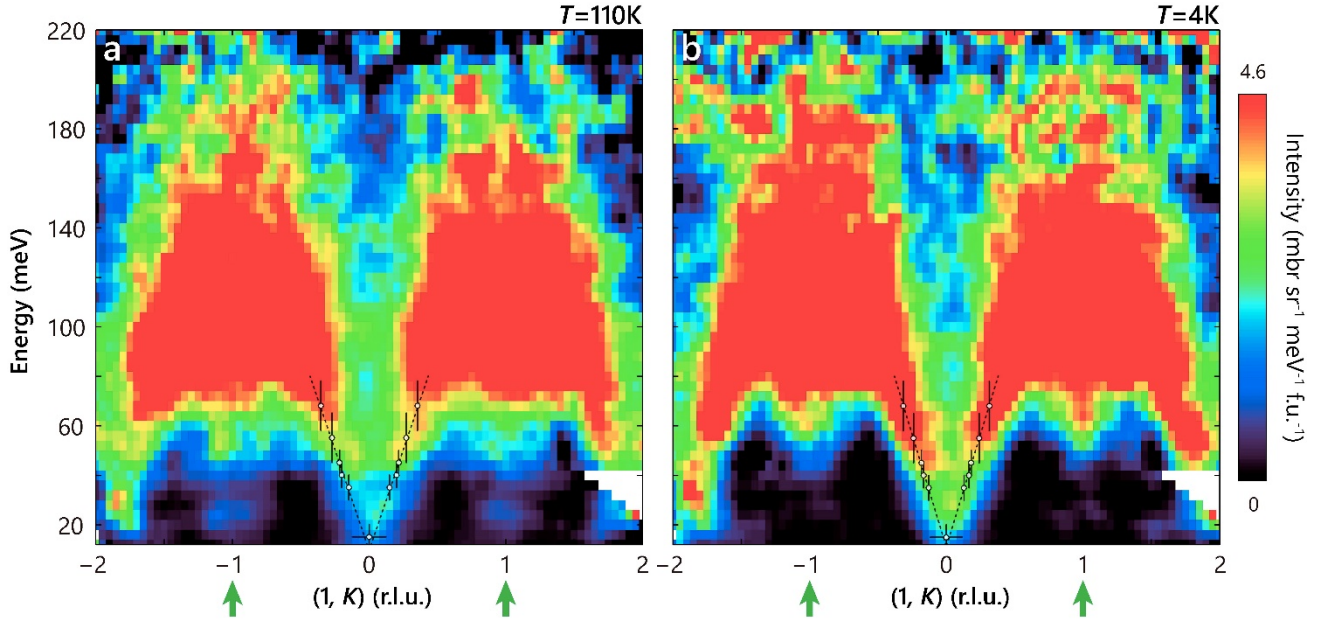
Figure 2 | Dispersions of the stripe and Néel spin fluctuations in FeSe at 4 and 110 K. Background-subtracted *E-K* slice of the spin fluctuations at various incident energies: **a**, *T* = 110 K; **b,** *T* = 4 K. The data at $E \geq 40$ and $E \leq 40$ meV were collected on ARCS by using incident energy of 294 and 79 meV, respectively. The isotropic Fe^{2+} magnetic form factor is corrected for both sets of data. The spectral weight transfer from the Néel (1, 1) to stripe (1, 0) wavevector below ~50 meV upon cooling to 4 K can be clearly seen. The open circles are dispersions obtained from the constant energy cuts below 68 meV in Fig. 3. The dashed lines are a guide to the eye.
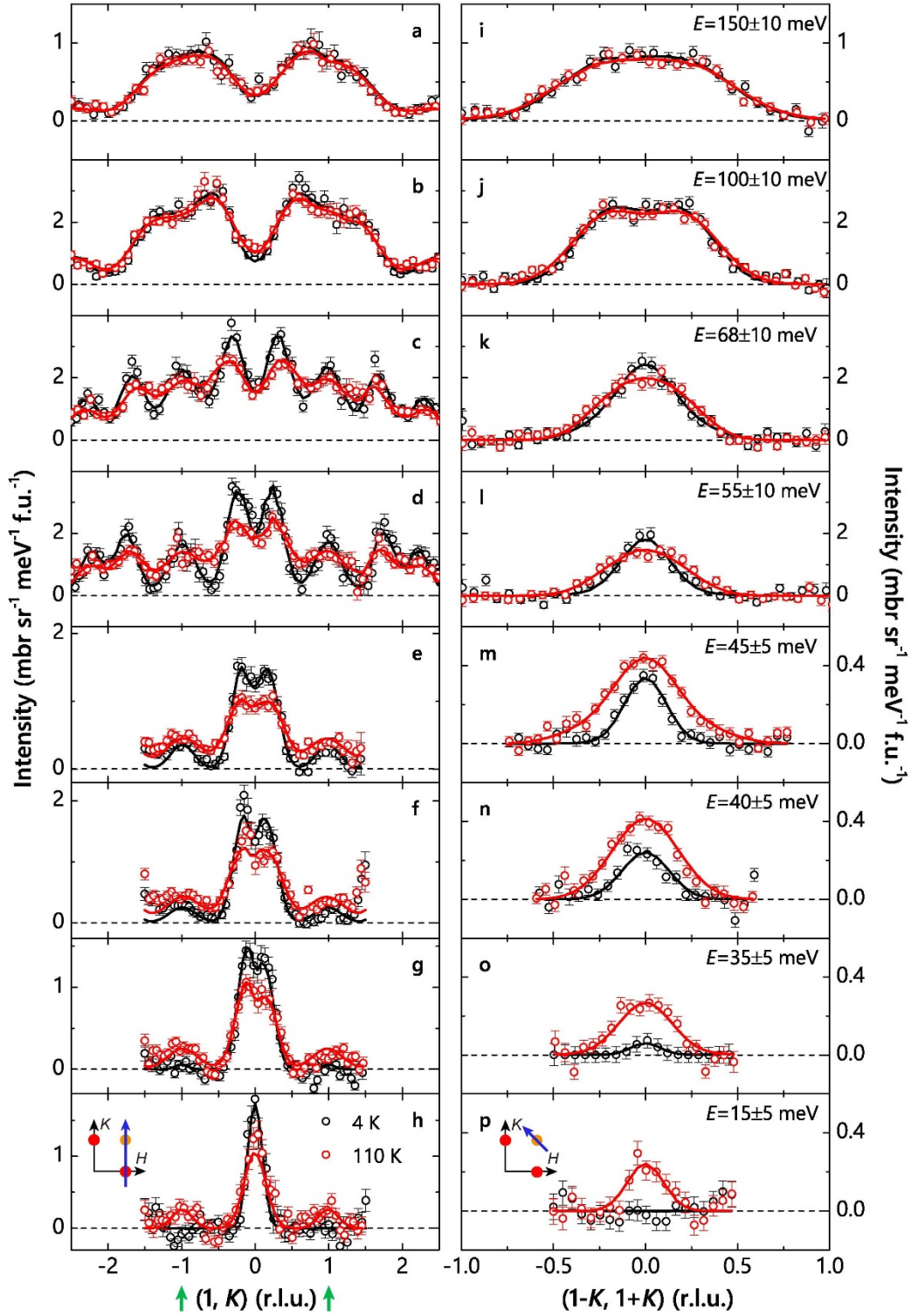
13

Figure 3 | Constant-energy cuts of the stripe and Néel spin fluctuations in FeSe at 4 K and 110 K. a-h, Background-subtracted constant-energy cuts through the stripe and Néel magnetic wavevectors along the K direction at 4 and 110 K. **i-p**, Background-subtracted constant-energy cuts through the Néel magnetic wavevector $\mathbf{Q} = (1, 1, L)$ along the transverse direction. The scan directions are marked by the arrows in the insets. The peak positions (dispersions) are determined by fitting with Gaussian profiles convoluted with the instrumental resolution, with the Fe^{2+} magnetic form factor corrected. The fitted dispersions are shown in Fig. 2. The error bars indicate one standard deviation.
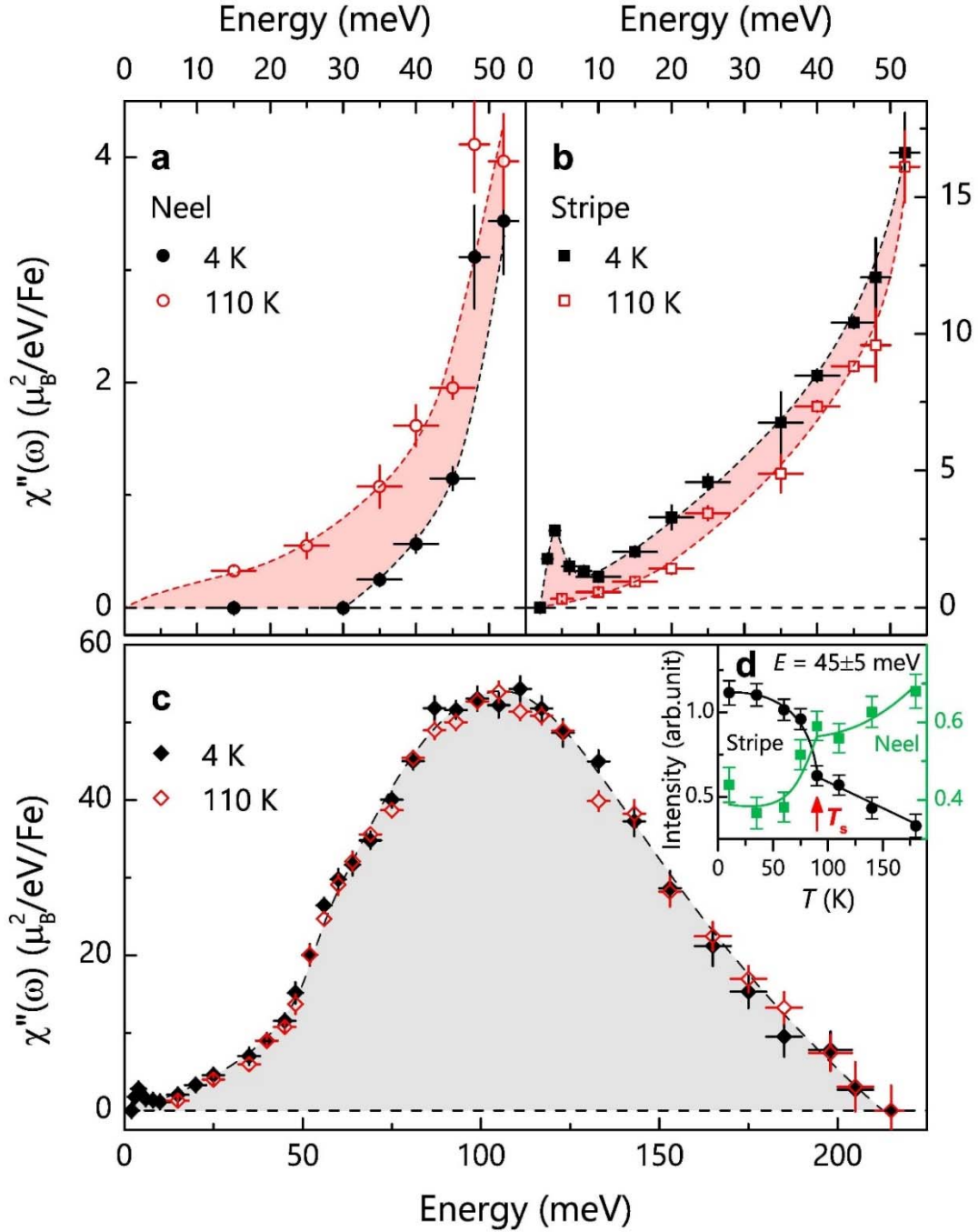
Figure 4 | Energy dependence of the local susceptibility χ″(ω) for FeSe at 4 and 110 K. a-c, Energy dependence of χ″(ω), at 4 and 110 K, calculated for (**a**) the Néel spin fluctuations, (**b**) the stripe spin fluctuations, and (**c**) the sum of the stripe and Néel spin fluctuations. A resonance mode is clearly observed at ~4 meV and 4 K (see Supplementary Information), whose intensity is consistent with the previous low energy measurements normalized with acoustic phonons[14]. **d**, Temperature dependence of the intensities of the stripe and Néel spin fluctuations. The data in (**a-c**) were collected on ARCS (incident energy E_i = 294, 79, 40 meV) and 4SEASONS (E_i = 21, 13.6 meV). The data in (**d**) were collected on MERLIN (E_i = 123.4 meV). The horizontal and vertical bars indicate the energy integration range and the statistical errors of one standard deviation, respectively.